Letter

Intrinsic charm quark valence distribution of the proton

Richard D. Ball,[1] Alessandro Candido,[2,3] Juan Cruz-Martinez,[3] Stefano Forte,[2] Tommaso Giani,[4,5] Felix Hekhorn,[2,6,7] Giacomo Magni,[4,5] Emanuele R. Nocera,[8] Juan Rojo,[4,5] and Roy Stegeman[1]

(NNPDF Collaboration)

[1]*The Higgs Centre for Theoretical Physics, University of Edinburgh, JCMB, KB, Mayfield Road, Edinburgh EH9 3JZ, Scotland*
[2]*Tif Lab, Dipartimento di Fisica, Università di Milano and INFN, Sezione di Milano, Via Celoria 16, I-20133 Milano, Italy*
[3]*CERN, Theoretical Physics Department, CH-1211 Geneva 23, Switzerland*
[4]*Department of Physics and Astronomy, Vrije Universiteit, NL-1081 HV Amsterdam, The Netherlands*
[5]*Nikhef Theory Group, Science Park 105, 1098 XG Amsterdam, The Netherlands*
[6]*University of Jyväskylä, Department of Physics, P.O. Box 35, FI-40014 University of Jyväskylä, Finland*
[7]*Helsinki Institute of Physics, P.O. Box 64, FI-00014 University of Helsinki, Helsinki, Finland*
[8]*Dipartimento di Fisica, Università degli Studi di Torino and INFN, Sezione di Torino, Via Pietro Giuria 1, I-10125 Torino, Italy*

(Received 26 October 2023; accepted 14 March 2024; published 1 May 2024)

We provide a first quantitative indication that the wave function of the proton contains unequal distributions of charm quarks and antiquarks, i.e., a nonvanishing intrinsic valence charm distribution. A significant nonvanishing valence component cannot be perturbatively generated; hence, our results reinforce previous evidence that the proton contains an intrinsic (i.e., not radiatively generated) charm quark component. We establish our result through a determination of the parton distribution functions of charm quarks and antiquarks in the proton. We propose two novel experimental probes of this intrinsic charm valence component: D-meson asymmetries in $Z + c$-jet production at the LHCb experiment and flavor-tagged structure functions at the Electron-Ion Collider.

DOI: 10.1103/PhysRevD.109.L091501

Introduction. The possible existence of charm quarks as intrinsic constituents of the proton, on the same footing as the much lighter up, down, and strange quarks, has fascinated physicists for more than four decades [1,2]. Charm quarks and antiquarks are heavier ($m_c \sim 1.5$ GeV) than the proton itself ($m_p \sim 1$ GeV). They are copiously pair-produced through the perturbative QCD radiation of gluons and light quarks that generates their scale dependence. An intrinsic charm (IC) component is the scale-independent result that is left after subtracting this radiative contribution.

A plethora of experimental and theoretical studies have tried to either identify or reject the presence of IC in the proton [3–6]. We have recently presented a determination of intrinsic charm in the proton from a global analysis of parton distribution functions (PDFs) [7–9]. This study found evidence for IC at the 3σ level and was supported by independent constraints from forward Z production with charm jets at the LHCb experiment [10].

In Ref. [9] we determined the distributions of charm quarks and antiquarks assuming equality of the intrinsic (scale-independent) charm and anticharm PDFs, i.e., the vanishing of the charm valence PDF

$$c^-(x, Q^2) = c(x, Q^2) - \bar{c}(x, Q^2). \tag{1}$$

The valence charm PDF $c^-(x, Q^2)$ must have vanishing integral over x at all scales Q^2, because the proton does not carry the charm quantum number, but the PDF itself may well be nonzero, as it happens for the strange valence PDF $s^- = s - \bar{s}$. Indeed, a nonvanishing charm valence component is always generated, like for any other quark flavor, by perturbative QCD evolution [11]. However, any perturbatively generated valence charm component is tiny in comparison to all other PDFs, including those of heavy quarks. Hence, any evidence of a sizable valence charm PDF is a

definite sign of its intrinsic nature. Model calculations [2,12], while in broad agreement on the shape of total IC PDF, widely differ in predictions for the shape and magnitude of the intrinsic valence charm component. Model calculations of IC complemented with input from lattice QCD [13] also predict a nonvanishing valence component.

Here we investigate this issue by performing a data-driven determination of the intrinsic valence charm PDF of the proton, based on the same methodology as in [9]. We generalize the NNPDF4.0 PDF determination by introducing an independent parametrization of the charm and anticharm PDFs, determine them from a global QCD analysis, and subtract the perturbatively generated contributions by transforming all PDFs to the three-flavor-number scheme (3FNS) in which perturbative charm vanishes so any residual charm PDF is intrinsic.

We find a nonzero charm valence PDF, with a positive valence peak for $x \sim 0.3$, whose local significance is close to two sigma. We demonstrate the stability of this result with respect to theoretical, dataset, and methodological variations. We then propose two novel experimental probes to further scrutinize this asymmetry between charm and anticharm PDFs: D-meson asymmetries in $Z + c$-jet production at LHCb [10,14] and flavor-tagged structure functions at the upcoming Electron-Ion Collider (EIC) [15,16].

Methodology. As in Ref. [9], we follow the NNPDF4.0 methodology, theory settings and dataset [8], the only modifications being related to the independent parametrization of the charm valence PDF. Firstly, the neural network architecture is extended with an additional neuron in the output layer in order to independently parametrize $c^-(x, Q_0)$, Eq. (1), at the PDF parametrization scale $Q_0 = 1.65$ GeV. In the default PDF basis ("evolution basis"; see Supplemental Material Appendix B [17]) this extra neuron is taken to parametrize the valence nonsinglet combination $V_{15} = (u^- + d^- + s^- - 3c^-)$, with $q^- \equiv q - \bar{q}$. In an alternative basis ("flavor basis") it instead parametrizes $\bar{c}$: so in both cases the valence component is obtained by taking linear combinations of the neural network outputs. In our previous analysis [8], the assumption of vanishing intrinsic valence was enforced by setting $V_{15} = V = \sum_i q_i^-$ in the evolution basis or $\bar{c} = c$ in the flavor basis at the scale Q_0.

In addition to experimental constraints, a nonzero charm valence must, as mentioned, satisfy the sum rule

$$Q_{15} \equiv \int_0^1 dx V_{15}(x, Q_0) = 3, \tag{2}$$

$$Q_c \equiv \int_0^1 dx (c - \bar{c})(x, Q_0) = 0, \tag{3}$$

in the evolution or flavor basis, respectively. This sum rule is enforced in the same manner as that of the strange valence sum rule [8]. Finally, to ensure cross-section positivity (at $Q^2 = 5$ GeV^2) separately for charm- and anticharm-initiated processes, we replace the neutral current F_2^c positivity observable (sensitive only to c^+) with its charged current counterparts F_2^{c,W^-} and $F_2^{\bar{c},W^+}$. The charm PDFs xc and $x\bar{c}$ themselves are not required to be positive definite [18–20]. Integrability and preprocessing are imposed as in NNPDF4.0. We have verified that results are stable upon repeating the hyperoptimization of all parameters defining the fitting algorithm, and thus we keep the same settings as in [8].

The valence charm pdf. As explained in Ref. [9], intrinsic charm is the charm PDF in the 3FNS, where charm is treated as a massive particle that does not contribute to the running of the strong coupling or the evolution of PDFs. In the absence of intrinsic charm ("perturbative charm" henceforth), the charm and anticharm PDFs in the 3FNS vanish identically. In the four-flavor-number scheme (4FNS), in which charm is treated as a massless parton, these PDFs are determined by perturbative matching conditions between the 3FNS and the 4FNS [21]. In our data-driven approach, the charm and anticharm PDFs, instead of being fixed by perturbative matching conditions, are determined from data on the same footing as the light quark PDFs. The deviation of data-driven charm from perturbative charm, i.e., in the 3FNS the deviation of the charm and anticharm PDFs from zero, is identified with the intrinsic component. In practice, we parametrize PDFs at $Q_0 = 1.65$ GeV in the 4FNS and then invert the matching conditions to determine the intrinsic component in the 3FNS.

In Fig. 1 we show xc^+ and xc^- in the 4FNS at $Q = 1.65$ GeV, i.e., just above the charm mass that we take to be $m_c = 1.51$ GeV, determined using next-to-next-to-leading-order (NNLO) QCD theory. The bands are 68% confidence level (C.L.) PDF uncertainties. We show both the purely perturbative and data-driven results, in the latter case both for $c = \bar{c}$ (same as in [9]) and $c \neq \bar{c}$. Note that the purely perturbative valence PDF vanishes at $Q = m_c$ at NNLO, and only develops a tiny component at one extra perturbative order (N^{3}LO) or at higher scales. Hence, a nonvanishing valence component in the 4FNS provides already evidence for intrinsic charm.

Upon allowing for a vanishing valence xc^- component, the total charm xc^+ is quite stable, especially around the peak at $x \sim 0.4$. This total charm PDF is also somewhat suppressed for smaller $x \lesssim 0.2$ as compared to the baseline result. In terms of fit quality, the χ^2 per data point for the global dataset decreases from 1.162 to 1.151, corresponding to an improvement by about 50 units in absolute χ^2. The main contributions to this decrease come from neutral current deep-inelastic scattering and LHC gauge boson production data (see Supplemental Material Appendix A [17]).

The valence component is nonzero and positive at more than one-sigma level in the $x \in [0.2, 0.4]$ region and consistent with zero within the large PDF uncertainties elsewhere. The size and shape of the valence charm PDF seen in Fig. 1 are stable upon variations of PDF

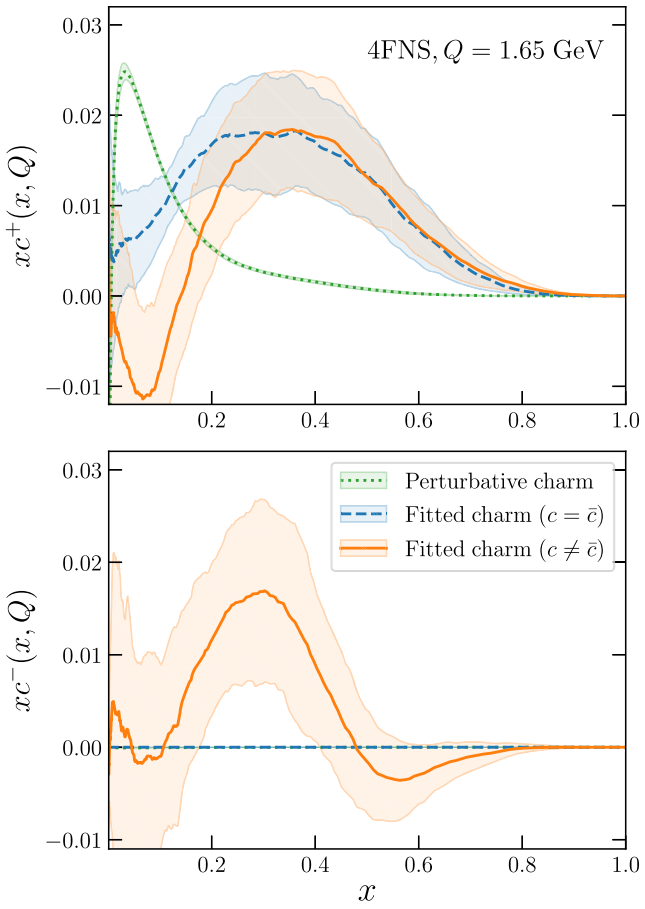

FIG. 1. The charm total xc^+ (top) and valence xc^- (bottom) PDFs in the 4FNS at $Q = 1.65$ GeV. The perturbative and data-driven results are compared, in the latter case either assuming $c^- = 0$ (as in [9]) or c^- determined from data.

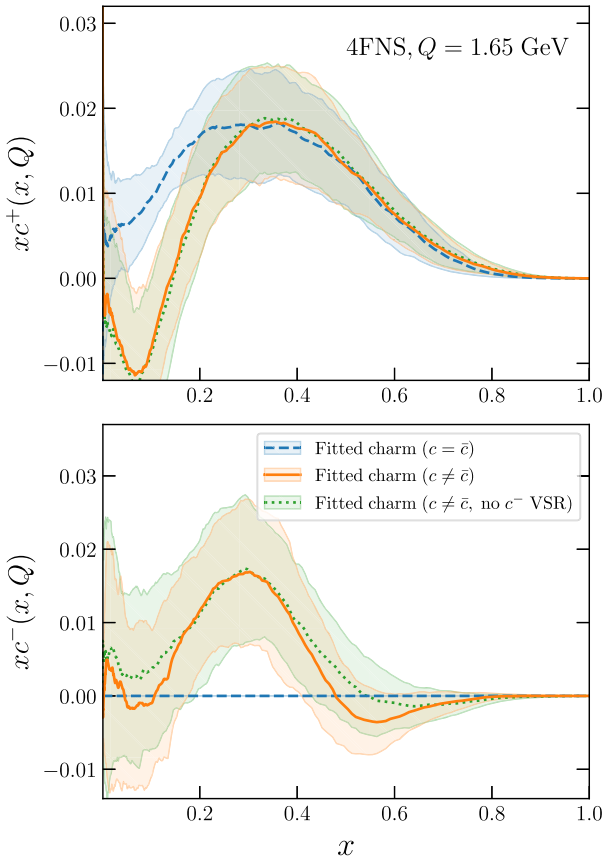

FIG. 2. The same as Fig. 2, now without imposing the charm valence sum rule Eq. (2) when $c \neq \bar{c}$.

parametrization basis (see Supplemental Material Appendix B [17]), the value of m_c (see Supplemental Material Appendix C [17]), the input dataset (see Supplemental Material Appendix D [17]), and the kinematic cuts in W^2 and Q^2 (see Supplemental Material Appendix E [17]). All other PDFs are mostly left unaffected by having allowed for a nonvanishing valence charm.

Whereas in our default determination we have imposed the charm valence sum rule Eq. (2), we have also repeated our determination without imposing this theoretical constraint. We then obtain $Q_c = 0.07 \pm 0.14$ and the resulting charm PDFs are shown in Fig. 2. This result demonstrates that the valence sum rule is actually enforced by the data, and our result is data driven.

Intrinsic valence charm. The intrinsic valence charm PDF is now determined by transforming back to the 3FNS scheme and is displayed in Fig. 3 (upper panel), together with its 4FNS counterpart already shown in Fig. 1. An estimate of the missing higher order uncertainties (MHOU) related to the truncation of the perturbative expansion is also included. This, as in [9], is estimated as the change in the 3FNS PDF when the transformation from the 4FNS to the 3FNS is performed to one higher perturbative order, i.e., N^{3}LO [22–30], as this is estimated to be the dominant missing higher order correction.

The 3FNS and 4FNS valence PDFs turn out to be quite close, implying that for the valence PDF, unlike for the total charm PDF, the theory uncertainty is smaller than the PDF uncertainty. We thus find that the intrinsic (3FNS) charm valence is nonzero and positive roughly in the same x region as its 4FNS counterpart.

The statistical significance of the nonvanishing valence is quantified by the pull, defined as the median PDF in units of the total uncertainty, shown in Fig. 3 (bottom). The local significance of the intrinsic valence is slightly below two sigma, peaking at $x \sim 0.3$. The significance of the total intrinsic component is similar to that found in Ref. [9], namely about three sigma for $x \sim 0.5$. As in Ref. [9], we also show the results found in fit variants including the F_2^c data measured by the European Muon Collaboration (EMC) [31] and the $Z + c$ data measured by the LHCb collaboration [10], both of which increase the local significance.

The results of Figs. 1–3 suggest that the intrinsic valence component may be nonzero, but their significance falls

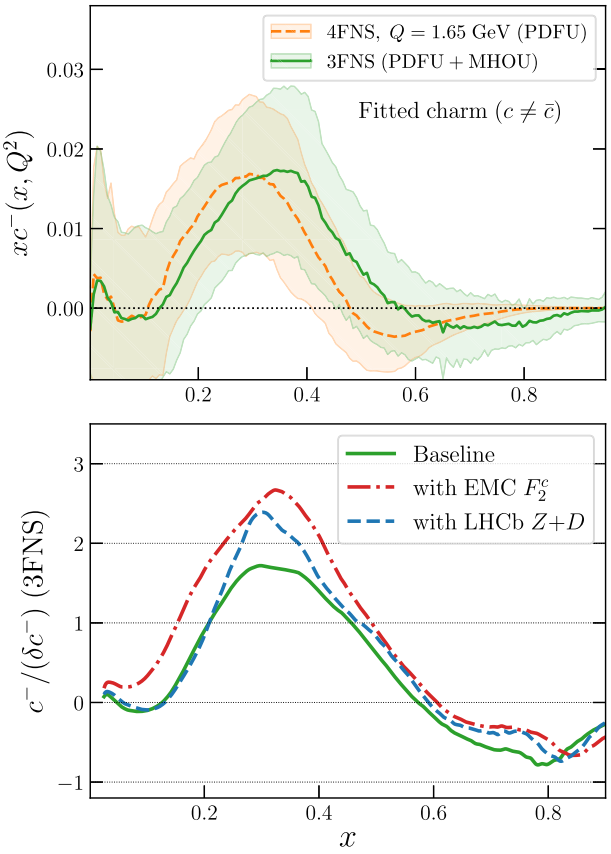

FIG. 3. Top: the 3FNS (intrinsic) valence charm PDF xc^-, compared to the 4FNS result (the same as Fig. 1 bottom). The 3FNS also includes MHOU due to the inversion from the 4FNS to the 3FNS. Bottom: the pull for valence xc^- charm PDF in the 3FNS. Results are shown both for the default fit and also when including the EMC F_2^c and LHCb $Z + c$ data.

below the three-sigma evidence level. We thus propose two novel experimental observables engineered to probe this valence charm component.

Charm asymmetries in $Z + c$ at LHC: The LHC run 2 data, which, as shown in Ref. [9], reinforce the evidence for an intrinsic total charm component, correspond to measurements of forward Z production in association with charm-tagged jets [10]. They are presented as a measurement of $\mathcal{R}_j^c(y_Z)$, the ratio between c-tagged and untagged jets in bins of the Z-boson rapidity y_Z, and they are obtained from tagging D mesons from displaced vertices. The higher statistics available first at runs 3 and 4 and later at the HL-LHC will enable the reconstruction of the exclusive decays of D mesons, and thus the separation of charm and anticharm-tagged final states. We thus define the asymmetry

$$\mathcal{A}_c(y_Z) \equiv \frac{N_j^c(y_Z) - N_j^{\bar{c}}(y_Z)}{N_j^c(y_Z) + N_j^{\bar{c}}(y_Z)}, \tag{4}$$

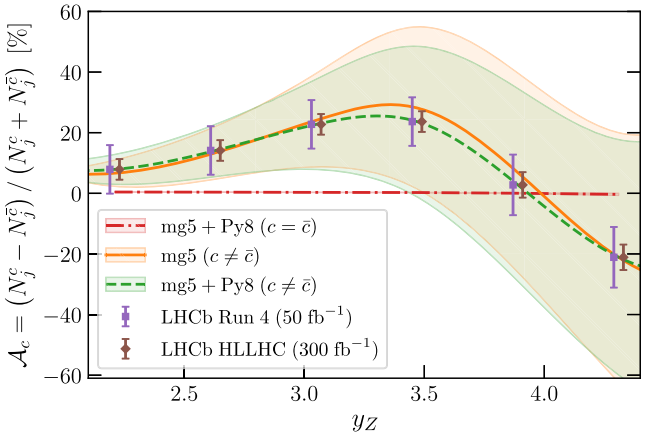

FIG. 4. The charm asymmetry $\mathcal{A}_c(y_Z)$, Eq. (4), in $Z + c$-jet production at LHCb ($\sqrt{s} = 13$ TeV) evaluated at LO matched to parton showers with the nonvanishing valence PDF determined here. The pure LO result and the result with vanishing charm valence are also shown for comparison. The bands correspond to one-sigma PDF uncertainties. Projected statistical uncertainties for LHCb measurements at run 4 ($\mathcal{L} = 50$ fb^{-1}) and the HL-LHC ($\mathcal{L} = 300$ fb^{-1}) are also shown.

where N_j^c ($N_j^{\bar{c}}$) is defined in the same manner as $\mathcal{R}_j^c$ [10], but now restricted to events with D mesons containing a charm quark (antiquark). This asymmetry is directly sensitive to a possible difference between the charm and anticharm PDFs in the initial state.

In Fig. 4 we display the asymmetry $\mathcal{A}_c(y_Z)$, Eq. (4), computed for $\sqrt{s} = 13$ TeV using the PDFs determined here, that allow for a nonvanishing valence component, as well as the default NNPDF4.0 with $c = \bar{c}$. Results are computed using MG5_aMC@NLO [32] at leading order (LO) matched to PYTHIA8 [33,34], with the same D-meson tagging and jet-reconstruction algorithm as in [10,14]. The leading-order parton-level result is also shown.

It is apparent from Fig. 4 that, even though the forward-backward asymmetry of the Z decay generates a small asymmetry $\mathcal{A}_c \neq 0$ even when $c = \bar{c}$ [35,36], the LO effect due to an asymmetry between c an $\bar{c}$ PDFs is much larger and stable upon showering and hadronization corrections. Indeed, higher-order QCD corrections largely cancel in the ratio $\mathcal{A}_c(y_Z)$.

In Fig. 4 we also display projected uncertainties for the LHCb measurement of this asymmetry at run 3 and at the HL-LHC (see Supplemental Material Appendix F [17] for details), showing that a valence component of the same size as our central prediction could be detected, respectively, at about a two-sigma or four-sigma level.

Charm-tagged Deep-Inelastic Scattering (DIS) at the EIC: A standard probe of the charm component of the proton is the deep-inelastic charm structure function F_2^c [31,37–39] and the associate deep-inelastic reduced charm production cross section $\sigma_{\rm red}^{\bar{c}c}$. Correspondingly, the charm valence can be determined from the reduced cross-section asymmetry

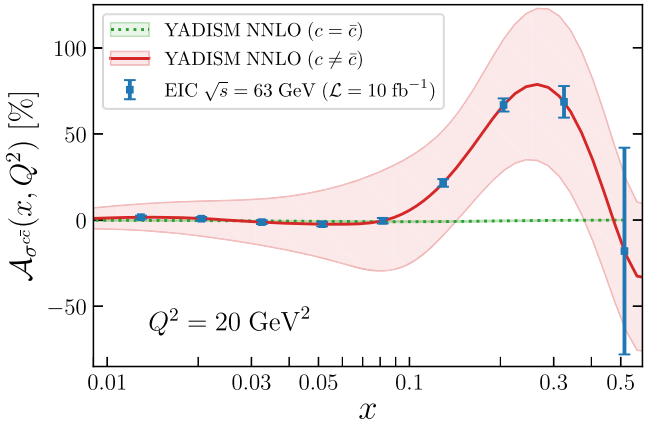

FIG. 5. The reduced charm-tagged cross-section asymmetry $\mathcal{A}_{\sigma^{c\bar{c}}}$, Eq. (5), at $Q^2 = 20$ GeV^2 computed at NNLO QCD using the nonvanishing valence PDF determined here. The result with vanishing charm valence is also shown for comparison. The bands correspond to one-sigma PDF uncertainties. The projected statistical uncertainties at the EIC [15] (running at $\sqrt{s} = 63$ GeV for $\mathcal{L} = 10$ fb^{-1}) are also shown.

$$\mathcal{A}_{\sigma^{c\bar{c}}}(x, Q^2) \equiv \frac{\sigma^{c}_{\rm red}(x, Q^2) - \sigma^{\bar{c}}_{\rm red}(x, Q^2)}{\sigma^{c\bar{c}}_{\rm red}(x, Q^2)}. \tag{5}$$

A measurement of this observable requires reconstructing final-state D mesons by identifying their decay products. At the future EIC this will be possible with good precision using the proposed ePIC detector [15,40,41].

The predicted asymmetry $\mathcal{A}_{\sigma^{c\bar{c}}}$ at $Q^2 = 20$ GeV^2 is shown in Fig. 5; results are shown at the reduced charm (parton) cross-section level, evaluated with YADISM [42] at NNLO accuracy. As in Fig. 4, we show results obtained both using the PDFs determined here, that allow for a nonvanishing valence component, as well as the default NNPDF4.0 with $c = \bar{c}$. We also display the projected statistical uncertainties [15] at the EIC running at $\sqrt{s} = 63$ GeV for $\mathcal{L} = 10$ fb^{-1} (see Supplemental Material Appendix E [17]). It is clear that a nonvanishing charm valence component can be measured at the EIC to very high significance even for a moderate amount of integrated luminosity.

In addition to the charm-tagged structure function $F_2^{c\bar{c}}$, at the EIC complementary sensitivity to the charm valence content of the proton would be provided by the charm-tagged parity-violating structure function $xF_3^{c\bar{c}}(x, Q^2)$. This observable has the advantage that at LO is already proportional to xc^- and, hence, provides a direct constraint on valence charm. Predictions for this observable are presented in Fig. 6. Even in the absence of detailed predictions for prospective EIC measurements of this observable, it is clear that its measurement would significantly constrain the charm valence PDF.

Outlook. Our main conclusion is that current experimental data provide support for the hypothesis that the valence charm PDF may be nonzero, even though with the NNPDF4.0 dataset it is not possible to reach three-sigma evidence. Whereas the situation may improve somewhat with future PDF determinations based on the full LHC run-3 dataset, dedicated observables such as the LHCb charm asymmetry Eq. (4) as well as charm production at the EIC Eq. (5) will be needed in order to achieve firm evidence or discovery. Other experimental probes that could be explored in this context include open charm production and asymmetries at the LHC, in particular for forward (LHCb [43,44]) and far-forward (FASERν [45], SND@LHC [46], and the Forward Physics Facility [47,48]) detectors. Progress in lattice computations might well also provide further constraints.

From the theory point of view, ongoing efforts toward a NNPDF determination based on N^{3}LO calculations should reduce some of the theory uncertainties affecting the current determination. On a more speculative vein, it might also be interesting to investigate an intrinsic bottom quark component and its eventual asymmetry.

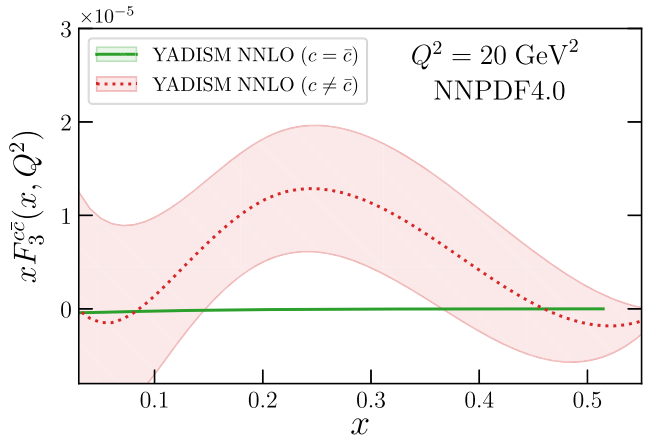

FIG. 6. The same as Fig. 5 for the charm-tagged parity-violating structure function $xF_3^{c\bar{c}}(x, Q^2)$ at the EIC (no projection for the statistical accuracy of the EIC measurement is available).

Acknowledgments. We are grateful to Rhorry Gauld for extensive discussions concerning $Z +$ charm production and to Reynier Cruz-Torres and Barak Schmookler for providing the EIC projections for F_2^c. We thank Thomas Boettcher, Dan Craik, Philip Ilten, Patrick Koppenburg, Niels Tuning, and Michael Williams, for information about the LHCb $Z +$ charm measurements and the associated projections. R. D. B. and R. S. are supported by the United Kingdom Science and Technology Facility Council (STFC) Grant No. ST/T000600/1. T. G. is supported by NWO (Dutch Research Council) via an ENW-KLEIN-2 project. F. H. is supported by the Academy of Finland Project No. 358090 and is funded as a part of the Center of Excellence in Quark Matter of the Academy of Finland, Project No. 346326. E. R. N. is supported by the Italian Ministry of University and Research (MUR) through the "Rita Levi-Montalcini" Program. J. R. and G. M. are partially supported by NWO (Dutch Research Council).

[1] S. J. Brodsky, P. Hoyer, C. Peterson, and N. Sakai, The intrinsic charm of the proton, Phys. Lett. B **93**, 451 (1980).

[2] S. J. Brodsky, A. Kusina, F. Lyonnet, I. Schienbein, H. Spiesberger, and R. Vogt, A review of the intrinsic heavy quark content of the nucleon, Adv. High Energy Phys. **2015**, 231547 (2015).

[3] P. Jimenez-Delgado, T. Hobbs, J. Londergan, and W. Melnitchouk, New limits on intrinsic charm in the nucleon from global analysis of parton distributions, Phys. Rev. Lett. **114**, 082002 (2015).

[4] R. D. Ball, V. Bertone, M. Bonvini, S. Carrazza, S. Forte, A. Guffanti, N. P. Hartland, J. Rojo, and L. Rottoli (NNPDF Collaboration), A determination of the charm content of the proton, Eur. Phys. J. C **76**, 647 (2016).

[5] M. Guzzi, T. J. Hobbs, K. Xie, J. Huston, P. Nadolsky, and C. P. Yuan, The persistent nonperturbative charm enigma, Phys. Lett. B **843**, 137975 (2023).

[6] T.-J. Hou, S. Dulat, J. Gao, M. Guzzi, J. Huston, P. Nadolsky, C. Schmidt, J. Winter, K. Xie, and C. P. Yuan, CT14 intrinsic charm parton distribution functions from CTEQ-TEA global analysis, J. High Energy Phys. 02 (2018) 059.

[7] R. D. Ball *et al.* (NNPDF Collaboration), An open-source machine learning framework for global analyses of parton distributions, Eur. Phys. J. C **81**, 958 (2021).

[8] R. D. Ball *et al.* (NNPDF Collaboration), The path to proton structure at 1% accuracy, Eur. Phys. J. C **82**, 428 (2022).

[9] R. D. Ball, A. Candido, J. Cruz-Martinez, S. Forte, T. Giani, F. Hekhorn, K. Kudashkin, G. Magni, and J. Rojo (NNPDF Collaboration), Evidence for intrinsic charm quarks in the proton, Nature (London) **608**, 483 (2022).

[10] R. Aaij *et al.* (LHCb Collaboration), Study of Z bosons produced in association with charm in the forward region, Phys. Rev. Lett. **128**, 082001 (2022).

[11] S. Catani, D. de Florian, G. Rodrigo, and W. Vogelsang, Perturbative generation of a strange-quark asymmetry in the nucleon, Phys. Rev. Lett. **93**, 152003 (2004).

[12] T. J. Hobbs, J. T. Londergan, and W. Melnitchouk, Phenomenology of nonperturbative charm in the nucleon, Phys. Rev. D **89**, 074008 (2014).

[13] R. S. Sufian, T. Liu, A. Alexandru, S. J. Brodsky, G. F. de Téramond, H. G. Dosch, T. Draper, K.-F. Liu, and Y.-B. Yang, Constraints on charm-anticharm asymmetry in the nucleon from lattice QCD, Phys. Lett. B **808**, 135633 (2020).

[14] T. Boettcher, P. Ilten, and M. Williams, Direct probe of the intrinsic charm content of the proton, Phys. Rev. D **93**, 074008 (2016).

[15] M. Kelsey, R. Cruz-Torres, X. Dong, Y. Ji, S. Radhakrishnan, and E. Sichtermann, Constraints on gluon distribution functions in the nucleon and nucleus from open charm hadron production at the Electron-Ion Collider, Phys. Rev. D **104**, 054002 (2021).

[16] R. Abdul Khalek *et al.*, Science requirements and detector concepts for the electron-ion collider: EIC Yellow Report, Nucl. Phys. **A1026**, 122447 (2022).

[17] See Supplemental Material at http://link.aps.org/supplemental/10.1103/PhysRevD.109.L091501 for details on the fit quality, on the dependence of results upon the parametrization basis, the value of m_c, the input dataset and the kinematic cuts in W^2 and Q^2, and on projected uncertainties for the Z+charm asymmetry data at LHCb and for the charm structure-function data at the EIC.

[18] A. Candido, S. Forte, and F. Hekhorn, Can $\overline{\text{MS}}$ parton distributions be negative?, J. High Energy Phys. 11 (2020) 129.

[19] J. Collins, T. C. Rogers, and N. Sato, Positivity and renormalization of parton densities, Phys. Rev. D **105**, 076010 (2022).

[20] A. Candido, S. Forte, T. Giani, and F. Hekhorn, On the positivity of MSbar parton distributions, arXiv:2308.00025.

[21] M. Buza and W. L. van Neerven, $O(\alpha_s^2)$ contributions to charm production in charged-current deep-inelastic lepton hadron scattering, Nucl. Phys. **B500**, 301 (1997).

[22] I. Bierenbaum, J. Blümlein, and S. Klein, The gluonic operator matrix elements at $O(\alpha_s^2)$ for DIS heavy flavor production, Phys. Lett. B **672**, 401 (2009).

[23] I. Bierenbaum, J. Blümlein, and S. Klein, Mellin moments of the $O(\alpha_s^3)$ heavy flavor contributions to unpolarized deep-inelastic scattering at $Q^2 \gg m^2$ and anomalous dimensions, Nucl. Phys. **B820**, 417 (2009).

[24] J. Ablinger, J. Blümlein, S. Klein, C. Schneider, and F. Wissbrock, The $O(\alpha_s^3)$ massive operator matrix elements of $O(n_f)$ for the structure function $F_2(x, Q^2)$ and transversity, Nucl. Phys. **B844**, 26 (2011).

[25] J. Ablinger, A. Behring, J. Blümlein, A. De Freitas, A. Hasselhuhn, A. von Manteuffel, M. Round, C. Schneider, and F. Wißbrock, The 3-loop non-singlet heavy flavor contributions and anomalous dimensions for the structure function $F_2(x, Q^2)$ and transversity, Nucl. Phys. **B886**, 733 (2014).

[26] J. Ablinger, J. Blümlein, A. De Freitas, A. Hasselhuhn, A. von Manteuffel, M. Round, and C. Schneider, The $O(\alpha_s^3 T_F^2)$ contributions to the gluonic operator matrix element, Nucl. Phys. **B885**, 280 (2014).

[27] A. Behring, I. Bierenbaum, J. Blümlein, A. De Freitas, S. Klein, and F. Wißbrock, The logarithmic contributions to the $O(\alpha_s^3)$ asymptotic massive Wilson coefficients and operator matrix elements in deeply inelastic scattering, Eur. Phys. J. C **74**, 3033 (2014).

[28] J. Ablinger, J. Blümlein, A. De Freitas, A. Hasselhuhn, A. von Manteuffel, M. Round, C. Schneider, and F. Wißbrock, The transition matrix element $a_{gq}(n)$ of the variable flavor number scheme at $o(\alpha_s^3)$, Nucl. Phys. **B882**, 263 (2014).

[29] J. Ablinger, A. Behring, J. Blümlein, A. De Freitas, A. von Manteuffel *et al.*, The 3-loop pure singlet heavy flavor contributions to the structure function $F_2(x, Q^2)$ and the anomalous dimension, Nucl. Phys. **B890**, 48 (2014).

[30] J. Blümlein, J. Ablinger, A. Behring, A. De Freitas, A. von Manteuffel, C. Schneider, and C. Schneider, Heavy flavor Wilson coefficients in deep-inelastic scattering: Recent results, *Proc. Sci.* QCDEV2017 (2017) 031.

[31] J. J. Aubert *et al.* (European Muon Collaboration), Production of charmed particles in 250-GeV μ^+-iron interactions, Nucl. Phys. **B213**, 31 (1983).

[32] J. Alwall, R. Frederix, S. Frixione, V. Hirschi, F. Maltoni, O. Mattelaer, H.-S. Shao, T. Stelzer, P. Torrielli, and M. Zaro, The automated computation of tree-level and next-to-leading order differential cross sections, and their matching to parton shower simulations, J. High Energy Phys. 07 (2014) 079.

[33] T. Sjostrand, S. Mrenna, and P. Z. Skands, A brief introduction to PYTHIA8.1, Comput. Phys. Commun. **178**, 852 (2008).
[34] P. Skands, S. Carrazza, and J. Rojo, Tuning PYTHIA8.1: The Monash 2013 Tune, Eur. Phys. J. Appl. Phys. **74**, 3024 (2014).
[35] R. Gauld, U. Haisch, B. D. Pecjak, and E. Re, Beauty-quark and charm-quark pair production asymmetries at LHCb, Phys. Rev. D **92**, 034007 (2015).
[36] R. Gauld, U. Haisch, and B. D. Pecjak, Asymmetric heavy-quark hadroproduction at LHCb: Predictions and applications, J. High Energy Phys. 03 (2019) 166.
[37] S. Forte, E. Laenen, P. Nason, and J. Rojo, Heavy quarks in deep-inelastic scattering, Nucl. Phys. **B834**, 116 (2010).
[38] R. D. Ball, M. Bonvini, and L. Rottoli, Charm in deep-inelastic scattering, J. High Energy Phys. 11 (2015) 122.
[39] H. Abramowicz *et al.* (H1, ZEUS Collaborations), Combination and QCD analysis of charm and beauty production cross-section measurements in deep inelastic ep scattering at HERA, Eur. Phys. J. C **78**, 473 (2018).
[40] R. A. Khalek, J. J. Ethier, E. R. Nocera, and J. Rojo, Self-consistent determination of proton and nuclear PDFs at the Electron Ion Collider, Phys. Rev. D **103**, 096005 (2021).
[41] N. Armesto, T. Cridge, F. Giuli, L. Harland-Lang, P. Newman, B. Schmookler, R. Thorne, and K. Wichmann, Impact of inclusive electron ion collider data on collinear parton distributions, Phys. Rev. D **109**, 054019 (2024).
[42] A. Candido, A. Garcia, G. Magni, T. Rabemananjara, J. Rojo, and R. Stegeman, Neutrino structure functions from GeV to EeV energies, J. High Energy Phys. 05 (2023) 149.
[43] R. Aaij *et al.* (LHCb Collaboration), Open charm production and asymmetry in pNe collisions at $\sqrt{s_{\mathrm{NN}}} = 68.5$ GeV, Eur. Phys. J. C **83**, 541 (2023).
[44] R. Aaij *et al.* (LHCb Collaboration), First measurement of charm production in its fixed-target configuration at the LHC, Phys. Rev. Lett. **122**, 132002 (2019).
[45] H. Abreu *et al.* (FASER Collaboration), First direct observation of collider neutrinos with FASER at the LHC, Phys. Rev. Lett. **131**, 031801 (2023).
[46] R. Albanese *et al.* (SND@LHC Collaboration), Observation of collider muon neutrinos with the SND@LHC experiment, Phys. Rev. Lett. **131**, 031802 (2023).
[47] J. L. Feng *et al.*, The forward physics facility at the high-luminosity LHC, J. Phys. G **50**, 030501 (2023).
[48] J. M. Cruz-Martinez, M. Fieg, T. Giani, P. Krack, T. Mäkelä, T. Rabemananjara, and J. Rojo, The LHC as a neutrino-ion collider, arXiv:2309.09581.